Simulation of Dispersionless Injections and Drift Echoes of Energetic Electrons Associated with Substorms

Xinlin Li,[1] D. N. Baker,[1] M. Temerin,[2] G. D. Reeves,[3] R. D. Belian[3]

Abstract. The term "dispersionless injection" refers to a class of events which show simultaneous enhancement (injection) of electrons and ions with different energies usually seen at or near geosynchronous orbit. We show that dispersionless injection can be understood as a consequence of simple changes in the electric and magnetic fields by modeling an electron injection event observed early on January 10, 1997 by means of a test-particle simulation. The background magnetic field in the model is a basic dipole field which has been made asymmetrical with a compressed dayside and a weakened nightside. The transient fields, which propagate from the magnetotail toward the Earth, are modeled with only one component of the electric field which is westward and a consistent magnetic field. These fields are used to model the major features of a dipolarization process during a substorm onset. We follow the electrons using a relativistic guiding center code. Our simulation results, with an initial kappa electron energy flux spectrum, reproduce the observed electron injection and subsequent drift echoes and show that the energization of injected electrons is mainly due to betatron acceleration of the preexisting electron population at larger radial distances in the magnetotail by the transient fields.

Introduction

A common feature of magnetospheric substorms is the discrete injection of energetic electrons and ions of tens to hundreds keV usually observed at or near geosynchronous orbit [McIlwain, 1974]. Depending on the local time of the measurement, these injections can appear to be dispersionless, indicating that fluxes of electrons and ions of different energies are enhanced at the same time. Because of the intriguing characteristic of the simultaneous enhancements of electrons and ions with different energies and because of its intrinsic role in substorms, the dispersionless injection of particles and ions associated with substorms remains one of the

outstanding problems in the magnetospheric physics.

McIlwain [1974] proposed a so-called "injection boundary" model to interpret the observed dispersionless injections. The injection boundary model suggests that during the injection process a sharp spatial boundary is formed that separates the newly injected or energized plasma from the pre-existing, undisturbed plasma. This model has been further explored [e.g., Mauk and McIlwain, 1974; Konradi et al., 1975; Mauk and Meng, 1987]. Despite the fact that the injection boundary model is not an acceleration model, it has had some success in explaining the observations phenomenologically.

Another key observational characteristic of substorm injections was discussed by Moore et al. [1981]. They investigated injections using two radially displaced satellites: ATS-6 and SCATHA. They found that the appearance of dispersionless injections occurs earlier at the outer satellite than at the inner satellite in the same local time sector. This propagating particle enhancement feature was found to be associated with a similar propagating magnetic signature. Russell and McPherron [1973] reported the observation of the inward propagation of a compressed magnetic field configuration (i.e., more dipolar magnetic field) by comparing two satellites: ATS-1 and OGO 5. They estimated a propagation speed of 150 km/s between 9 and 6.6 R_E. To explain these observations, Moore et al. [1981] proposed an "injection front" model in which an injection corresponds to a compressional wave front that propagates earthward from a disturbance occurring in the magnetotail. Particles are transported toward the Earth by such a compressional wave. Betatron acceleration, by moving electrons and ions into stronger magnetic field, yields the necessary energization of the injected particles. The observational evidence for betatron acceleration of electrons by compressional waves associated with substorms had been discussed earlier [e.g., Kivelson et al., 1973].

Recently Reeves et al. [1996] studied the radial propagation of substorm injections using CRRES and LANL geosynchronous energetic particle data. They found that essentially all 29 cases they investigated were consistent with an inward/earthward propagation of the particle injections. The averaged propagation speed inside geosynchronous orbit was 24 km/s.

More recently Birn et al. [1997, 1998] have investigated both proton and electron acceleration and injections on the basis of geosynchronous observations and of test-particle orbits in the

dynamic fields of a three-dimensional MHD simulation of magnetotail neutral line formation and dipolarization. Their test particle simulation can explain major features of the initial rise of the particle injection at geosynchronous orbit. They found most energization occurs due to betatron acceleration as particles are transported into a strong magnetic field region by a time dependent electric field, predominantly in the dawn-to-dusk directions. However, their simulation box was restricted in the nightside (5–25 R_E) and did not produce the complete temporal evolution of the injected particles to compare with the observations. From these simulation and from observations near geosynchronous orbit [Shepherd et al., 1980; Aggson et al., 1983; Rowland and Wygant, 1998], it is clear that the driving force of the injections must be the transient electric fields, pointing predominantly in the dawn-to-dusk or westward directions when close to the magnetic equatorial plane.

To understand how these transient electric fields accelerate particles and produce dispersionless injections near geosynchronous orbit, we simulate an injection by tracing particles under analytical model fields. The time varying fields in our model propagate toward the Earth from the magnetotail and represent the major feature of a dipolarization process at a substorm onset [Baker et al., 1996]. Such a test particle simulation can help us understand how electric and magnetic fields change during substorm onset.

We illustrate our model by simulating an electron injection observed early on January 10, 1997. We will address the following questions: (1) Where do the electrons come from? (2) Is it necessary to invoke the injection boundary model to explain the observed dispersionless injections? and (3) What is the cause of the often observed double-peak structure (a dip or dips within the first enhancement) of injected electrons [Belian et al.,1984]?

Model

Our model fields are similar to the ones in Li et al. [1993], which were developed to model the sudden compression of the magnetosphere by a strong interplanetary shock. Here, however, the time varying fields are instead associated with a dipolarization, during which the northward magnetic field in the magnetic equatorial plane increases due to a temporally and spatially varying electric field predominantly pointing westward. In our model the perturbed

fields propagate from the tail toward the Earth. The electric field is modeled as a time dependent Gaussian pulse with a purely azimuthal electric field component that propagates radially inward at a constant velocity, decreases away from midnight, and is partially reflected near the plasmapause. The modeled magnetic field dipolarization which is determined from Faraday's law occurs first at longitude ϕ_0 (midnight) and subsequently at other longitudes. Explicitly, in the usual spherical coordinates (r, θ, ϕ), where r is measured from the center of the Earth, and $\phi = 0°$ is at local noon, positive eastward, the electric field is given [Li et al., 1993] by:

$$\mathbf{E}_w = -\hat{e}_\phi E_0 (1 + c_1 \cos(\phi - \phi_0))^p \left[\exp(-\xi^2) - c_2 \exp(-\eta^2) \right], \quad (1)$$

where the terms in the square brackets are associated respectively with the incoming pulse and reflecting pulse. In (1) $\xi = [r + v_0(t - t_{ph})]/d$, $\eta = [r - v_0(t - t_{ph}) - r_d)]/d$, v_0 is the pulse propagation speed, and d is the width of the pulse; $c_1(> 0)$ and $p(> 0)$ describe the local time dependence of the electric field amplitude, which is largest at ϕ_0; $t_{ph} = t_i + (c_3 R_E/v_0)(1 - \cos(\phi - \phi_0))$ represents the delay of the pulse from ϕ_0 to other local times; c_3 determines the magnitude of the delay; c_2 determines the partial reflection of the pulse; $r_d = 7R_E$ indicates that the reflection occurs at $r = 3.5R_E$; and t_i determines the location of the pulse at the start of the simulation. In this letter we present results with E_0=0.5 mV/m, $c_1 = 1., c_2 = 0.4, c_3 = 4.0, p = 3, \phi_0 = 180°$, v_0=100 km/s, t_i=2550 s, and d=16,000 km.

The magnetic field of the pulse, $\mathbf{B}_w$, is obtained from Faraday's law and satisfies $\mathbf{E}_w \cdot (\mathbf{B}_E + \mathbf{B}_w)$=0 and $\bigtriangledown \cdot (\mathbf{B}_E + \mathbf{B}_w)$=0, where $\mathbf{B}_E$ is the Earth's background time independent magnetic field, which is stronger on the dayside and weaker on the nightside.

This asymmetric background magnetic field is achieved by sending a pulse field, similar to the one described above but starting from noon and with no reflection into a reduced dipole field ($B_0 = 31000 \times 0.7$ nT at the equator of the surface of the Earth) (E_0=2.22 mV/m, $c_1 = -1., c_2 = 0, c_3 = 0.4, p = 1, \phi_0 = 0°$, v_0=100 km/s, t_i=-2550 s, and d=16,000 km). This gives rise to a strengthed dayside and weakened nightside magnetic field. In the simulation, the background magnetic field at the equator, for example, at geosynchronous orbit (6.6 R_E) is 105 nT at local noon, 75 nT at midnight, and 90 nT at dawn and dusk. These values are comparable to average GOES-8 and GOES-9 magnetic field measurements [H. Singer, private

comm., 1998].

Figure 1 shows the time-dependent fields in the equatorial plane (where $B_z = -B_\theta$) at geosynchronous orbit. There is a decay of the fields away from midnight to simulate a dipolarization that usually occurs within a limited local time zone [Baker et al., 1996].

We superpose this time varying field on the background magnetic field and follow electrons using a relativistic guiding center approximation for electrons with $v_{||} = 0$, [Northrop, 1963]

$$\dot{W} = q\dot{\mathbf{R}}_\perp \cdot \mathbf{E}_w + \frac{M_r}{\gamma}\frac{\partial B}{\partial t}, \tag{2}$$

$$\dot{\mathbf{R}}_\perp = \frac{\hat{e}_1}{B} \times (-c\mathbf{E}_w + \frac{M_r c}{\gamma e} \bigtriangledown B), \tag{3}$$

where $\dot{\mathbf{R}}_\perp$ describes the guiding center motion perpendicular to the instantaneous magnetic field $\mathbf{B} = \mathbf{B}_E + \mathbf{B}_w$, $\hat{e}_1 = \mathbf{B}/B$ is a unit vector along $\mathbf{B}$, $\gamma = (W + m_0c^2)/m_0c^2$ is the relativistic energy factor, W is the electron's kinetic energy, $M_r = p_\perp^2/2m_0B$ is the relativistic first adiabatic invariant and $p_\perp$ is the electron's perpendicular momentum.

Results and Discussions

Figure 2 shows the guiding center trajectory of two electrons with 90° pitch angle at the equator. One has an initial condition of $r_0 = 12R_E$, $W_0 = 26$ keV, and $\phi_0 = 120°$ (red) and the other has $r_0 = 14R_E$, $W_0 = 25$ keV, and $\phi_0 = 135°$ (green). The wave pulse starts at about $40R_E$ from midnight at $t = 0$. Before the arrival of the wave field, the electron only performs a gradient-B drift, whose velocity is energy-dependent. When the wave arrives, the electron encounters an oppositely-directed magnetic field gradient due to the wave field, which can reduce or even reverse the local magnetic field gradient, such that the electron can drift in the opposite direction (westward). Meanwhile, each electron also moves radially inward because of the $\mathbf{E} \times \mathbf{B}$ drift, which is energy-independent. As each electron moves closer to the Earth, the background magnetic field starts to dominate and the electron again drifts eastward. As soon as the wave fields are no longer present, the electrons perform only a gradient-B drift but in a stronger magnetic field region (closer to the Earth).

Figure 3 shows the time history of radial distance and kinetic energy of the electrons in Fig 2. Taking the "red" electron as an example, before encountering the wave fields, the

electron performs only a gradient-drift motion along the contour of a constant background magnetic field, which is stronger on the dayside and weaker on the nightside. During this time its energy is conserved. After the electron encounters the incoming wave fields at $t = 25$ min, marked by the dashed line, it moves quickly inward and is energized to 160 keV. Later the electron also encounters the partially reflected wave fields (in which the electric field is reversed, pointing eastward) at $t = 38.5$ min, marked by the dotted line, and moves outward and is de-energized (W drops to 136 keV). After $t = 50$ min, marked by the dash-dot line, when the wave fields are gone, the electron performs only gradient drift motion again but with a net energy gain of 110 keV. The "green" electron encounters the wave fields a little earlier because it is initially farther out and happens to encounter less of the reflected wave field and has a net energy gain of 199 keV (final W=224 keV).

To compare with observed dispersionless injections, we need to perform a multi-particle calculation. Fig. 4 represents such a comparison. The left column is an example of an energetic electron injection observed by Los Alamos National Laboratory (LANL) sensors (omni-directional) on three satellites at geosynchronous orbit with a time resolution is 10 s [Belian et al., 1992]. The injected electrons detected by spacecraft 1990-095 appear dispersionless. As these electrons drift, they were detected by spacecraft 1991-080, but by this time they start to show some dispersion as more energetic electrons arrive earlier. Even later, they were detected by spacecraft 1994-084 with more dispersion. The same population of electrons continued to drift around the earth and was detected by the three spacecraft again despite some losses or new injections. This feature is a called a "drift echo event" [Lanzerotti et al., 1967]. The right column shows our simulation, in which the detectors' responses and actual location and motion have been incorporated. The dispersionless feature, drift echo, double-peak feature, even the width and shape of the fluxes are more or less reproduced.

In order to simulate the electron distribution, we followed 777,690 electrons as they drifted in the combined pulse and background fields, recording their energy, arrival time, radial distance, and initial conditions as they pass various local times. We distributed initial test-particle electrons in the equatorial plane at distances from r=5–16.95R_E in increments of 0.05 R_E, in azimuth every 5°, and at energies between 10 and 662.64 keV in increments of 1%. All

electrons had 90° pitch angles. In the post-processing stage each electron was given a weight which depended on the assumed initial distribution in energy and radial distance [Li et al., 1993]. The initial energy distribution was a kappa distribution [Vasyliunas, 1968] with $\kappa = 3$ and $E_0 = 0.5$ keV. These parameters are typical for a moderately active plasma sheet [Christon et al., 1991] and similar to the ones used by Birn et al. [1998]. The initial radial dependence was given by

$$fr = [\frac{(r_0 - a_0)^{nl}}{r_0^{ml}}]/[\frac{(a_{0d} - a_0)^{nl}}{a_{0d}^{ml}}], \tag{4}$$

where $a_0 = 3, nl = 6, ml = 10, a_{0d} = 6$, and

$$fr = fr * \exp(-r_0^2/7.5^2) \tag{5}$$

when r_0 is greater than 12 R_E. Thus, given an initial electron distribution, we can obtain electron fluxes and distributions at any location and time and can compare the simulation results with the LANL observations. The electron fluxes were summed over $\pm 0.2 R_E$ at r=$6.6 R_E$ and plotted with a time resolution of 51 s. The electron fluxes were also given a 3-hour e-folding time decay to simulate the loss after the injection. There are no new injections in the simulation. The small fluctuations in the simulated results are due to the statistics of the finite number of electrons. The simulated injection occurs approximately 14 minutes after the pulse passes 20 R_E. Substorm effects are thought to propagate somewhat faster from 20 R_E to 6.6 R_E. In our model, we use a constant pulse propagation velocity of 100 km/s, which is a compromise between the faster propagation speeds at larger radial distances and the smaller propagation speeds at smaller radial distances [Reeves et al., 1996]

The initial radial distribution for the simulation in Fig. 4 is given by (4) and (5) and displayed as the red shade area in (a1) of Fig. 5. Panel (a2) of Fig. 5 is the simulation result at spacecraft 1990-095 using the same fields but with an extra initial distribution shown as the green shade area in (a1) of Fig. 5. With these additional electrons the dips between the "double peaks" in (a1) of Fig. 4 are mostly filled. In order to determine the initial radial location of the electrons that contribute to the injected flux, we can divide the initial distribution and show only the electrons which had certain initial radial distances. In (b1) and (b2) of the Fig. 5 we show electrons with initial $r_0 < 11 R_E$ and $r_0 \geq 11 R_E$ respectively. We see a more obvious double-

peak feature in (b1), which is in fact a common feature in observations. These comparisons suggest that the double-peak features such as those shown in (a1) of Fig. 4 is due to the lack of electrons with appropriate initial energies at larger radial distances. We can further separate the initial radial distribution in our simulation and obtain the results shown in (c1), (c2), (d1), and (d2). It is clear that the injected electrons mostly come from farther out. More than 90% of the enhancement is due to electrons originally from $r_0 \geq 9R_E$. On the other hand, electrons initially located closer to geosynchronous orbit contribute to the initial enhancement. The observed dispersionlessly-injected electrons at geosynchronous orbit come originally from a continuous spatial region: mostly from a few R_E away but a smaller part originate within a couple of R_E as well. Since we have achieved good agreement with data without invoking an injection boundary model, these results suggest that there is no need to impose such an model to explain the observed dispersionless injections.

Whether of not dispersion is seen in the initial rise of the electron flux depends on whether the incoming pulse or the gradient drift dominates the changes in the electron flux. At midnight (or the local time centered on the direction of the pulse arrival) the pulse moves all energy particles inward simultaneously and thus no dispersion is seen in the initial rise of the electron flux. At other local times the higher energy electrons already affected by the pulse at midnight may arrive before the pulse itself or the pulse may be weak away from midnight. In this case the gradient drift will dominate and dispersion will be seen in the initial arrival of electrons of different energy. The same considerations apply to ions except that ions drift in the opposite direction.

Summary and Conclusions

Dispersionless injections can be understood as a consequence of a simple model of transient electric and magnetic fields associated with dipolarization during a substorm. When an electron encounters the propagating fields, its gradient-B drift is dominated by the transient magnetic field and its $\mathbf{E_w} \times \mathbf{B}$ motion, which is energy-independent, is directed toward the Earth. The betatron acceleration by the transient fields leads to energization of the electron. While our model of the transient fields is simple, it likely represents the components that are

most responsible for the energization and transport of the electrons.

Based on our simulation results, we conclude:

(1) the source of electrons in dispersionless injections at geosynchronous orbit is mostly from more than a few R_E away. Electrons which originate closer make a smaller contribution but produce the initial enhancement.

(2) There is no spatial boundary in the initial electron distribution. The dispersionless injection is caused by an electric field and a self-consistent magnetic field that propagates through the plasma, convecting the plasma inward. Thus there is no need to invoke an "injection boundary" to explain the observed dispersionless injection unless the electric field itself is considered a "boundary" but it moves and passes through the plasma.

(3) The often-observed double-peak feature in the first peak of a drift-echo event is due to the decrease in the appropriate phase space density of electrons at large radial distances [Li et al., 1993], which suggests that the plasma distribution in the magnetotail is usually, neither spatially nor temporally, uniform.

Though our perturbation field model, which consists of only one component of the electric field, is only designed to have the necessary electrodynamics to explain dispersionless injections and drift echoes, the model, nevertheless, implicitly contains much of the phenomenology often mentioned in the description of the onset of substorms in the magnetotail [Baker et al., 1996]. From Faraday's law we can calculate the corresponding perturbation in the magnetic field. The perturbation in the magnetic field consists of an increase followed by decrease but with the net result that after the perturbation is over the magnetic field is larger. The analogous effect during substorms is called a "dipolarization" since by increasing the northward component of the magnetic field the dipolarization makes the magnetic field at the equator more like an unperturbed dipole field. Though we don't need to calculate the perpendicular current for our test particle simulations, by using Ampere's law and assuming no variations in the 'z' direction we can determine the perpendicular current in the equatorial plane. This current also fluctuates but the net result is a current in the direction opposite to the normal cross-tail current. The analogous effect during substorms is called a "current disruption". Though field-aligned currents are not part of the model, the electric field in the model should map to the

ionosphere where part of the current should close. The analogous effect during substorms is called the "diversion of the cross-tail current". This field-aligned current is presumably carried by Alfven waves which are thought also to be responsible for the Pi2 waves seen at substorm onset. In the model at any given radial distance the perturbation starts first at midnight and later spreads in azimuth in both directions. The analogous effect during substorms is called the "expansion of the substorm current wedge". From the electric and magnetic fields in the model we can calculate the $\mathbf{E} \times \mathbf{B}$ convective flow. Had we chosen a faster propagation velocity farther out in the magnetosphere, the $\mathbf{E} \times \mathbf{B}$ convective velocity would have been faster and could have been called a "bursty bulk flow". In the model the $\mathbf{E} \times \mathbf{B}$ velocity is, however, only about 70 km/s but in the data flows over 1000 km/s have been seen in the magnetotail [Fairfield et al., 1998].

Thus our model, simple as it is, allows us to picture many of the phenomena thought to occur at substorm onset in the magnetotail. By varying parameters or superimposing impulses, many different possible fluctuations can be modeled. However one should also realize that there is little plasma physics in the model. The only plasma effect comes from the small propagation velocity of the assumed perturbation since in vacuum a electromagnetic perturbation would propagate at the speed of light. The assumed constant velocity in the model is approximately equivalent to assuming a constant magnetosonic velocity. Thus we cannot comment on the initiation of substorms on the basis of the model. However, the model is consistent with the idea that a perturbation farther out in the magnetotail propagates inward, perhaps in the form of "bursty bulk flows", and produces a dipolarization and other associated phenomena, including dispersionless injections, seen at the radial distance corresponding to geosynchronous orbit.

Acknowledgments.

The work at University of Colorado was supported by NSF grant ATM-9624390 and NASA grant NAG5-4896, NAG5-7112.

References

Aggson, T. L., J. P. Heppner, and N. C. Maynard, Observations of large magnetospheric electric fields during the onset phase of a substorm, *J. Geophys. Res.*, *88*, 3981, 1983.

Baker, D. N., T. I. Pulkkinen, V. Angelopoulos, W. Baumjohann, and R. L. McPherron, Neutral line model of substorms: Past results and present view, *J. Geophys. Res.*, *101*, 12975, 1996.

Belian, R. D., D. N. Baker, E. W. Hones, and P. R. Higbie, High-energy proton drift echoes: multiple peak structure, *J. Geophys. Res.*, *89*, 9101, 1984.

Belian, R. D., G. R. Gisler, T. E. Cayton, and R. Christensen, High-Z energetic particles at geosynchronous orbit during the great solar proton event series of October 1989, *J. Geophys. Res.*, *97*, 16897, 1992.

Birn, J., M. F. Thomsen, J. E. Borovsky, G. D. Reeves, D. J. McComas, R. D. Belian, and M. Hesse, Substorm ion injections: Geosynchronous observations and test particle orbits in three-dimensional dynamics MHD fields, *J. Geophys. Res.*, *102*, 2325, 1997.

Birn, J., M. F. Thomsen, J. E. Borovsky, G. D. Reeves, D. J. McComas, R. D. Belian, and M. Hesse, Substorm electron injections: Geosynchronous observations and test particle simulations, *J. Geophys. Res.*, *103*, 9235, 1998.

Christon, S. P., D. J. Williams, and D. G. Mitchell, Spectral characteristics of plasma sheet ion and electron populations during disturbed geomagnetic conditions, *J. Geophys. Res.*, *96*, 1, 1991.

Fairfield, D., et al., Geotail observation of substorm onset in the inner magnetotail, *J. Geophys. Res.*, *103*, 103, 1998.

Kivelson, M. G., T. A. Farley, and M., P. Aubry, *J. Geophys. Res.*, , *76*, 3079, 1973.

Konradi, A., C. L. Semar, and T. A. Fritz, Substorm-injected protons and electrons and the injection boundary model, *J. Geophys. Res.*, *80*, 543, 1975.

Lanzerotti, L. J., C. S. Roberts, and W. L. Brown, Temporal variation in the electron flux at synchronous altitude, *J. Geophys. Res.*, *72*, 5893, 1967.

Li, X., I. Roth, M. Temerin, J. Wygant, M. K. Hudson, and J. B. Blake, Simulation of the prompt energization and transport of radiation particles during the March 23, 1991 SSC,

Geophys. Res. Lett., *20*, 2423, 1993

Northrop, T. G., The adiabatic motion of charged particles. Interscience Publishers, New York, 1963.

Mauk, B. H., and C. E. McIlwain, Correlation of Kp with the substorm injected plasma boundary, *J. Geophys. Res.*, *79*, 3193, 1974.

Mauk, B. H., and C.-I. Meng, Plasma injection during substorms, *Physica Scripta, T18*, 128, 1987.

McIlwain, C. E., Substorm injection boundaries, *Magnetospheric Physics*, edited by B. M. McCormac, p. 143, D. Reidel, Hingham, Mass., 1974.

Moore, T. E., R. Arnoldy, J. Feynmann, and D. A. Hardy, Propagating substorm injection fronts, *J. Geophys. Res.*, *86*, 6713, 1981.

Reeves, G. D., R. W. H. Friedel, M. G. Henderson, A. Korth, P. S. McLachlan, and R. D. Belian, Radial propagation of substorm injections, International Conference on Substorms-3, *ESA SP-339*, 579-584, 1996.

Rowland, D. and J. R. Wygant, The dependence of the large scale electric field in the inner magnetosphere on magnetic activity, *J. Geophys. Res.*, in press, 1998.

Russell, C. T., and R. L. McPherron, The magnetotail and substorms, *Space Sci. Rev.*, *15*, 205, 1973.

Shepherd, G. G., R. Bostrom, H. Derblom, C.-G. Falthammar, R. Gendrin, K. Kaila, A. Korth, A. Pedersen, R. Pellinen, and G. Wrenn, Plasma and field signatures of poleward propagating auroral precipitation observed at the foot of the Geos 2 field line, *J. Geophys. Res.*, *85*, 4587, 1980.

Vasyliunas, D. J., A survey of low-energy electrons in the evening sector of the magnetosphere with OGO 1 and OGO 3, *J. Geophys. Res.*, *73*, 2839, 1968.

D. N. Baker and X. Li, LASP/CU, 1234 Innovation Dr., Boulder, CO 80303-7814; e-mail: lix@kitron.colorado.edu

Laboratory for Atmospheric and Space Physics, University of Colorado, Boulder

M. Temerin, SSL, University of California, Berkeley, CA 94720

R. D. Belian and G. D. Reeves, Mail Stop D-436, Los Alamos National Laboratory, Los Alamos, NM 87545

(Received _____)

[1]Lab. for Atmospheric and Space Physics, University of Colorado, Boulder

[2]Space Sciences Lab., University of California, Berkeley

[3]Los Alamos National Lab., Los Alamos, New Mexico

Figure Captions

Figure 1. Modeled electric field, E_ϕ, and magnetic field, B_z, in the equatorial plane at geosynchronous orbit at different locations.

Figure 2. Trajectory of two electrons initially placed at the equatorial plane with $r_0 = 12R_E$, $W_0 = 26$ keV, and $\phi_0 = 120°$ (red) and $r_0 = 14R_E$, $W_0 = 25$ keV, and $\phi_0 = 135°$ (green).

Figure 3. Radial distance and kinetic energy time history of the two electrons in Fig. 2.

Figure 4. Differential fluxes of electrons: from LANL observations in the early Jan. 10, 1997 in left column and simulation results in right column

Figure 5. (a1) initial radial distribution display, the red shade area comes from eqs. 4 and 5 and is the initial radial distribution for the simulation in Fig. 4; the red shade plus the green shade comes from eq. 4 only and is the initial radial distribution for the simulation for (a2), at 1990-095 spacecraft position. The rest of panels are simulation results from designated regions (as labeled) of the same initial distributions.

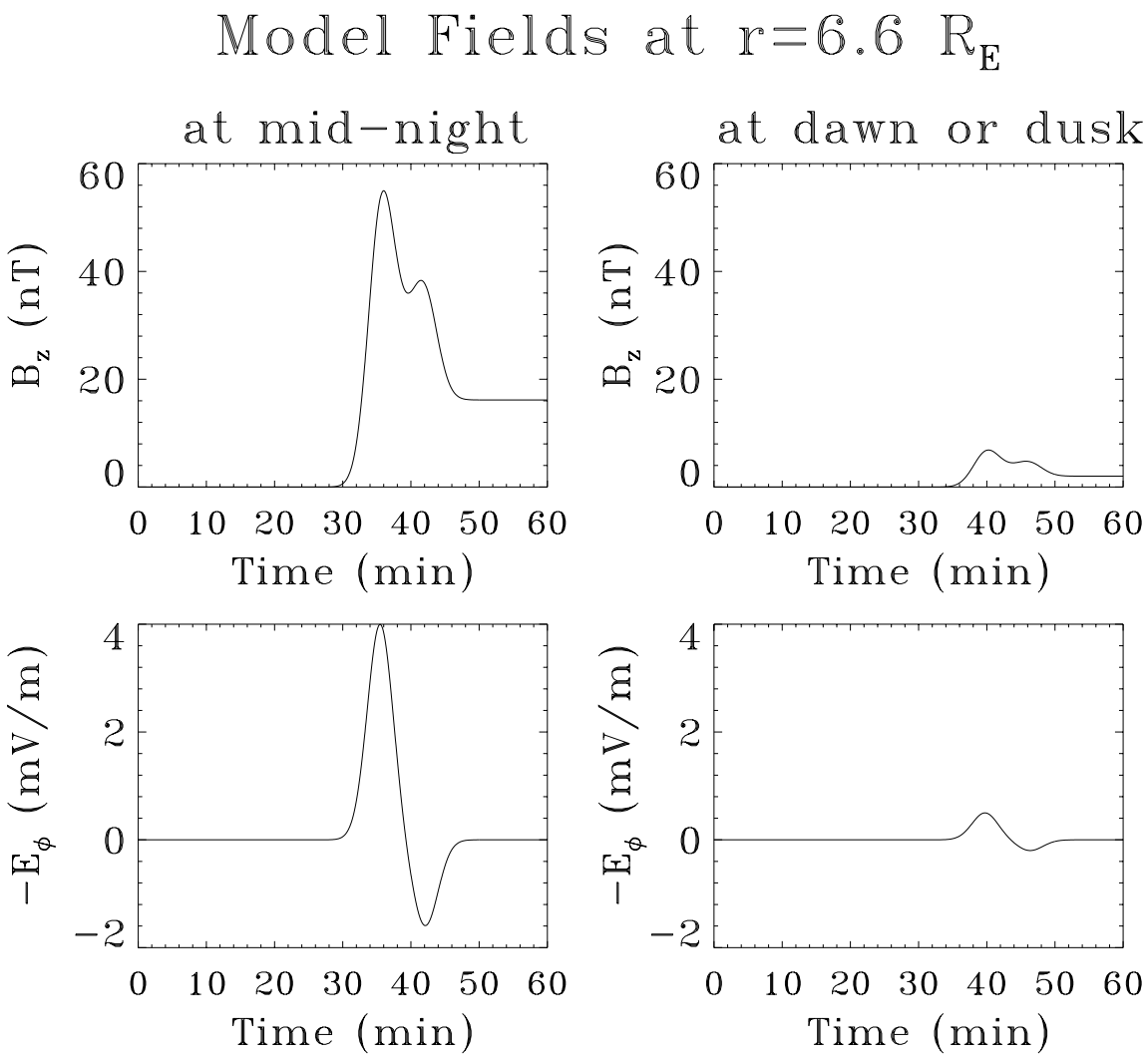
Model Fields at r=6.6 R_E
at mid−night
at dawn or dusk
B_z (nT)
$-E_\phi$ (mV/m)
Time (min)
0
10
20
30
40
50
60
0
20
40
60
−2
2
4

Figure 1

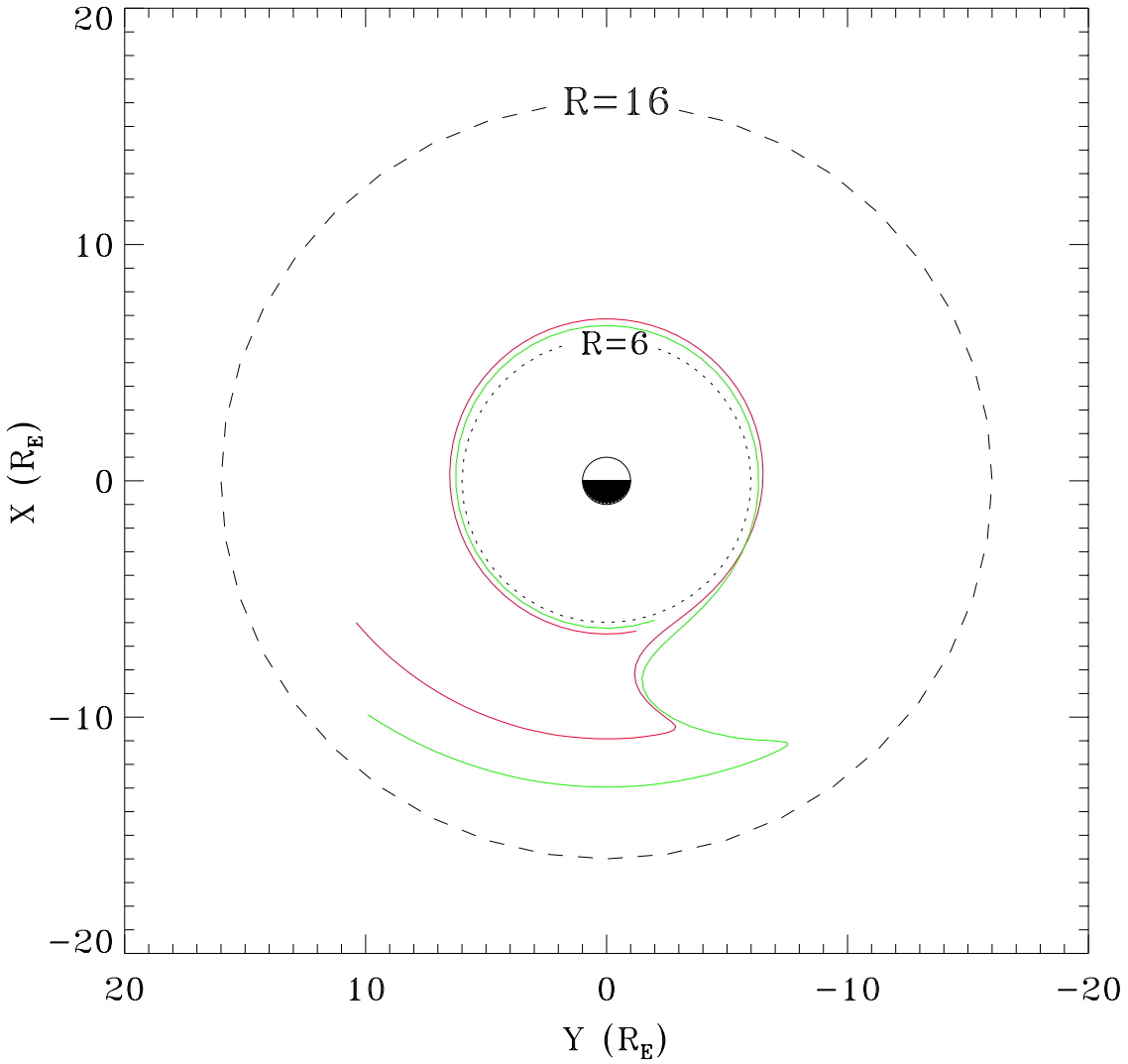

Figure 2

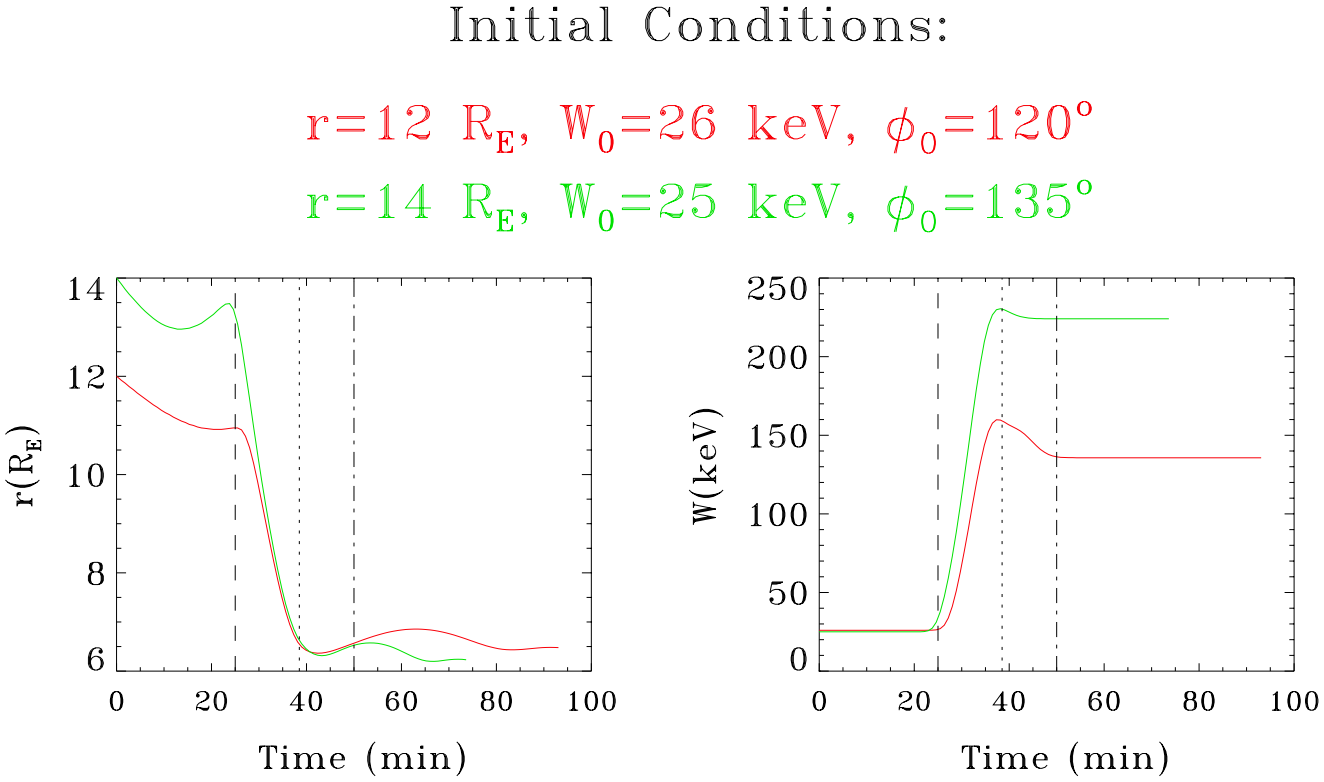
Initial Conditions:
r=12 R_E, W_0=26 keV, φ_0=120°
r=14 R_E, W_0=25 keV, φ_0=135°
r(R_E)
14
12
10
8
6
0
20
40
60
80
100
Time (min)
W(keV)
250
200
150
100
50
0
0
20
40
60
80
100
Time (min)

Figure 3

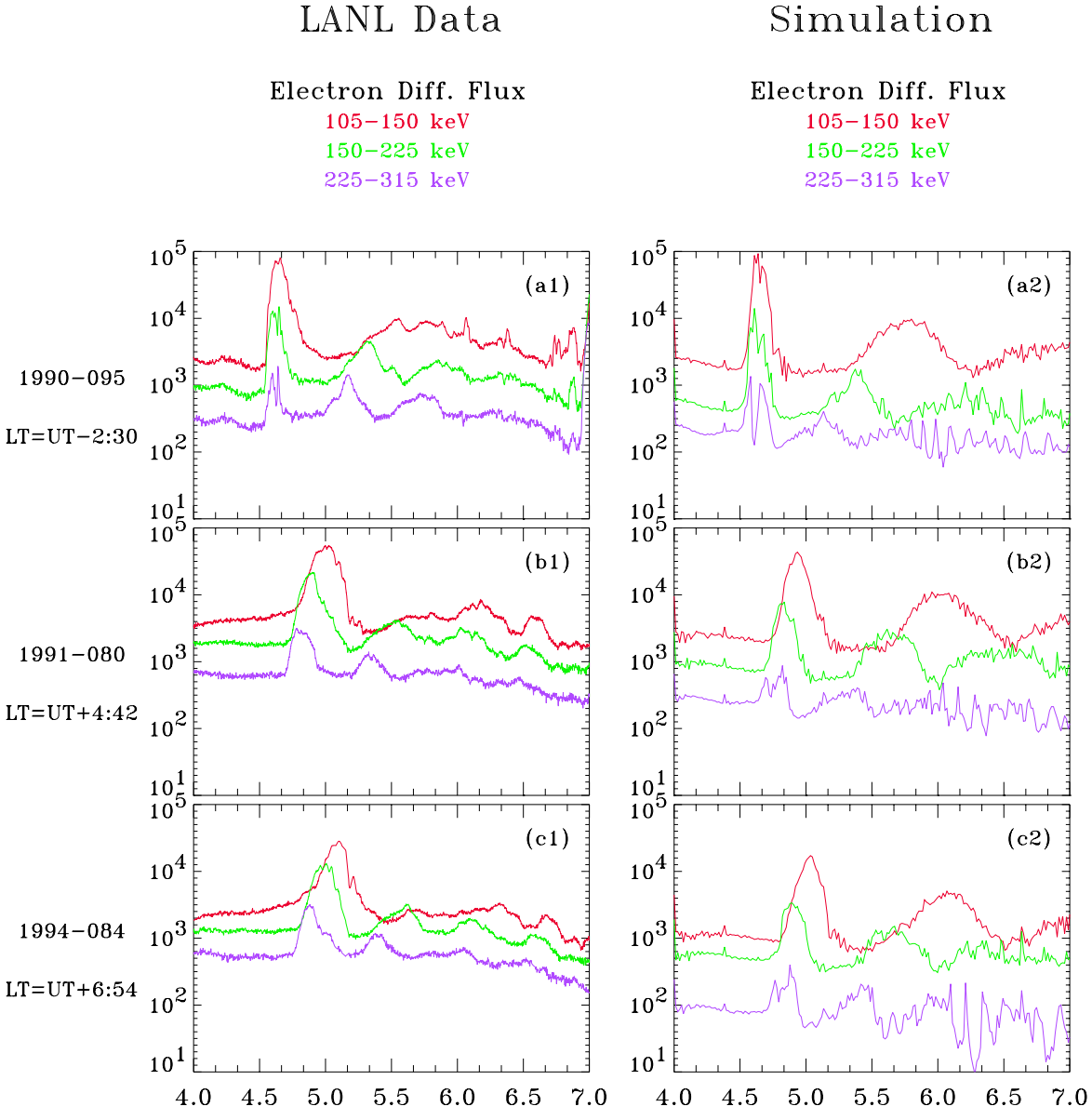
LANL Data
Simulation
Electron Diff. Flux
105–150 keV
150–225 keV
225–315 keV
Electron Diff. Flux
105–150 keV
150–225 keV
225–315 keV
(a1)
(a2)
(b1)
(b2)
(c1)
(c2)
1990–095
LT=UT–2:30
1991–080
LT=UT+4:42
1994–084
LT=UT+6:54
10^1
10^2
10^3
10^4
10^5
4.0
4.5
5.0
5.5
6.0
6.5
7.0
UT (hour) starting on Jan. 10, 1997

Figure 4

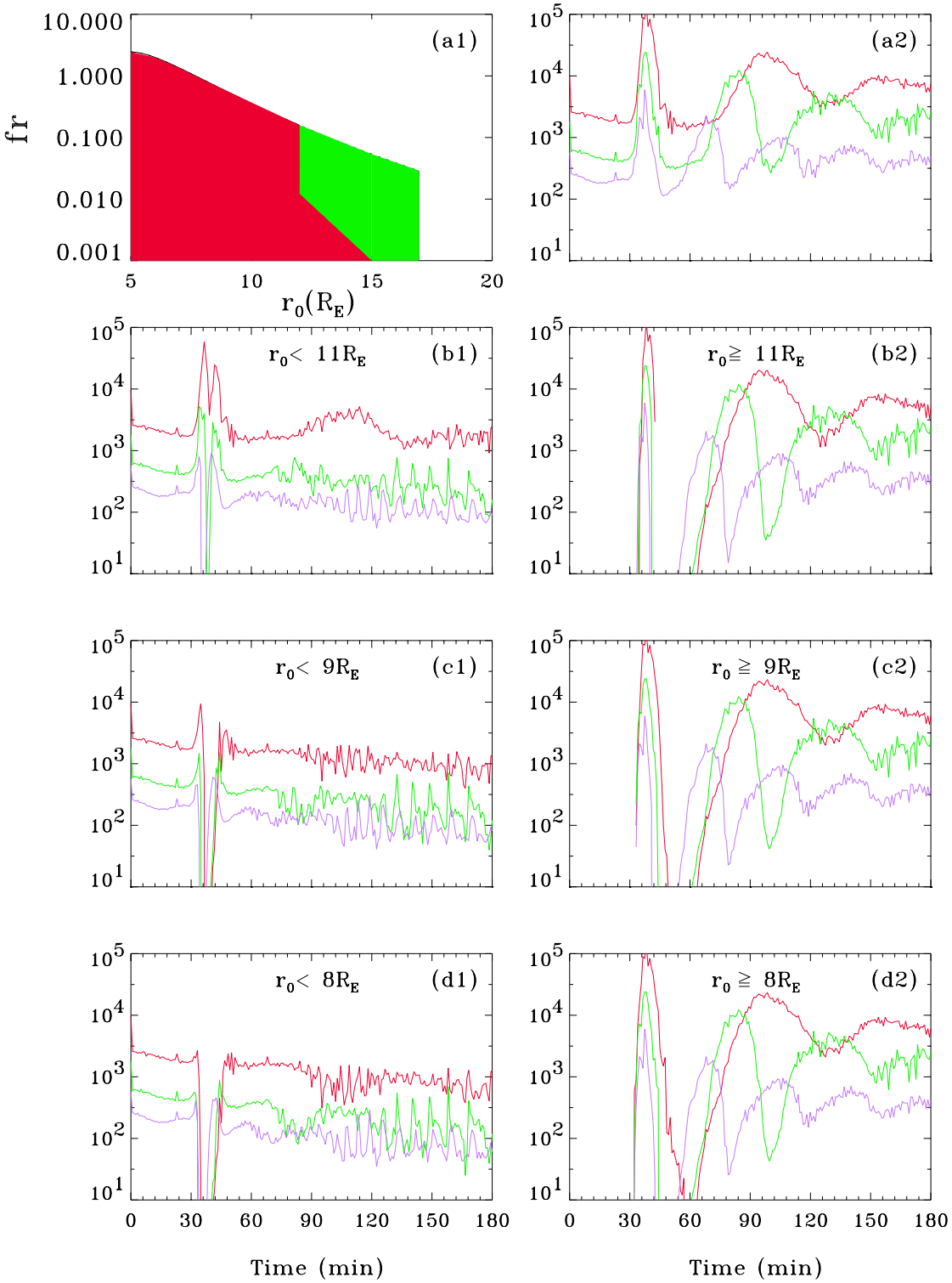
(a1)
(a2)
(b1)
(b2)
(c1)
(c2)
(d1)
(d2)
fr
10.000
1.000
0.100
0.010
0.001
5
10
15
20
r0(RE)
r0< 11RE
r0≧ 11RE
r0< 9RE
r0 ≧ 9RE
r0< 8RE
r0 ≧ 8RE
10^5
10^4
10^3
10^2
10^1
0
30
60
90
120
150
180
Time (min)
Time (min)

Figure 5